THE PROTEIN SOCIETY   WILEY

Solution X-ray scattering highlights discrepancies in *Plasmodium* multi-aminoacyl-tRNA synthetase complexes

José R. Jaramillo Ponce | Anne Théobald-Dietrich | Philippe Bénas |
Caroline Paulus | Claude Sauter | Magali Frugier [ORCID]

Université de Strasbourg, CNRS,
Architecture et Réactivité de l'ARN, UPR
9002, Strasbourg, France

Correspondence
José R. Jaramillo Ponce and Magali
Frugier, Université de Strasbourg, CNRS,
Architecture et Réactivité de l'ARN, UPR
9002, Strasbourg F-67084, France.
Email: j.jaramillo@ibmc-cnrs.unistra.fr
and m.frugier@ibmc-cnrs.unistra.fr

Abstract

tRip is a tRNA import protein specific to *Plasmodium*, the causative agent of malaria. In addition to its membrane localization and tRNA trafficking properties, tRip has the capacity to associate with three aminoacyl-tRNA synthetases (aaRS), the glutamyl- (ERS), glutaminyl- (QRS), and methionyl- (MRS) tRNA synthetases. In eukaryotes, such multi-aaRSs complexes (MSC) regulate the moonlighting activities of aaRSs. In *Plasmodium*, tRip and the three aaRSs all contain an N-terminal GST-like domain involved in the assembly of two independent complexes: the Q-complex (tRip:ERS:QRS) and the M-complex (tRip: ERS:MRS) with a 2:2:2 stoichiometry and in which the association of the GST-like domains of tRip and ERS (tRip-N:ERS-N) is central. In this study, the crystal structure of the N-terminal GST-like domain of ERS was solved and made possible further investigation of the solution architecture of the Q- and M-complexes by small-angle x-ray scattering (SAXS). This strategy relied on the engineering of a tRip-N-ERS-N chimeric protein to study the structural scaffold of both *Plasmodium* MSCs and confirm the unique homodimerization pattern of tRip in solution. The biological impact of these structural arrangements is discussed.

KEYWORDS
aminoacyl- synthetase-interacting multifunctional proteins (AIMP), aminoacyl-tRNA synthetase, GST-like domain, multi-aminoacyl-tRNA synthetase complex (MARS/MSC), Plasmodium, protein complex, RNA binding protein, tRip, tRNA

1 | INTRODUCTION

Aminoacyl-tRNA synthetases (aaRSs) are a family of essential enzymes that ensure the correct attachment of an amino acid to its cognate tRNAs. (Rubio Gomez & Ibba, 2020) In eukaryotes, a subset of cytosolic aaRSs is organized into a multi-synthetase complex (MSC) built on aaRS-interacting multifunctional proteins (AIMPs) (reviewed in Guo & Yang, 2013; Laporte et al., 2014; Havrylenko & Mirande, 2015). AaRSs and AIMPs are moonlighting proteins and participate in translation while located inside the MSC (Deinert et al., 2001; Kang et al., 2012; Kyriacou & Deutscher, 2008) and to a wide range of non-translational functions activated by their

(a) Q-complex / M-complex
QRS-N / MRS-N
ERS-N
tRip-N
EMAPII-like

(b)

β1 α1 β2 β3

```
tRip-N  MG-----CTLNLVEN-DIKSDILKLALDFIKTNIVENDDN---------VVFPEIKYGQ---------------KISYEHN  50
ERS-N   MGIKDSKINIYYGKNY---PFLCRTVFNIYQNNIK-KKTANNLNDKKIKEICVNFINDKT-----------VVEDIKVEFV  65
QRS-N   MG--EHVEKIYIKNTS-DLGNEFFYFYNWIK-----------------EKFNISLI--------INESNSLRHNIVLELS  51
MRS-N   MG------ILYPNKYLLSGTLKCMLAAHIYK----------------LPLELSDDFFFTRTFEIDKSLIVNKKPLLIYE  56
```

β4 α2 α3

```
tRip-N  -------------KKTYKE----FFCSLYAIIDTY----------NCYSQFFC-----------ENEDKVSESEEFIFNLA  102
ERS-N   RNTVSDQTRKNTNTNNSVTSS--DKIFAINLDFLL-----------KTNLYYFTSYRENINRNIITNVFFQAQYNEWIDFLR  134
QRS-N   -----------EGNNISLNELNSCEVIFHIIRNSHNKKDNWGNEFENEQDVEE-----------N-PFKIVQIEELKQFLK  109
MRS-N   --------------NKFVSS---TNAICFLFHRL----------KNKGINTKG-----------LD-DKLRLYLTWIEWSD  98
```

α4 α5

```
tRip-N  SDKFKL-------KPLDMKHLNDILRE----------------------RSYIVSDKHASLVDIFYFCCVYKILK---PM  141
ERS-N   NKDIE------KNIIPICEHINKHLYL----------------------NTFLSFHYLTLSDIYIYYEMHKYFSGNITT  185
QRS-N   NILL----QKKKLENDFFEKIENEMIKK----------------------NNNIFAKDKLRYVDFLLFCILKKNKI---EK  161
MRS-N   ILEKNIEHLNKKKIIESLDLLESYLSENNNKKFICDEVDQIKREDGCNGANQNPKNGICGITLADIYVYTSLKYSNI---VI  177
```

α6 α7 α8

```
tRip-N  TAKEKVEYYHICRWYIHLQETL-ICDFVKLHKLDIRSGVESLLNSGIVTCTNEKASNEQVGS----202-----(GTSGLVPR)  210
ERS-N   NLKYPKQYKNINRWFRLIKALLHDHVATDA------ELIQNLKVKEKI------------------227-(FIDGGSSGLVPR)  239
QRS-N   -I-NPK-YENLNNWFLKNNIS-----------------------------------------179---(SIASENLYFQ)  189
MRS-N   -C-NES-WSHINSYVERINNL--EDVQKV----VEAVEKVHKLKNIYSLFISKTCEKNIN------228-----(ASENLYFQ)  236
```

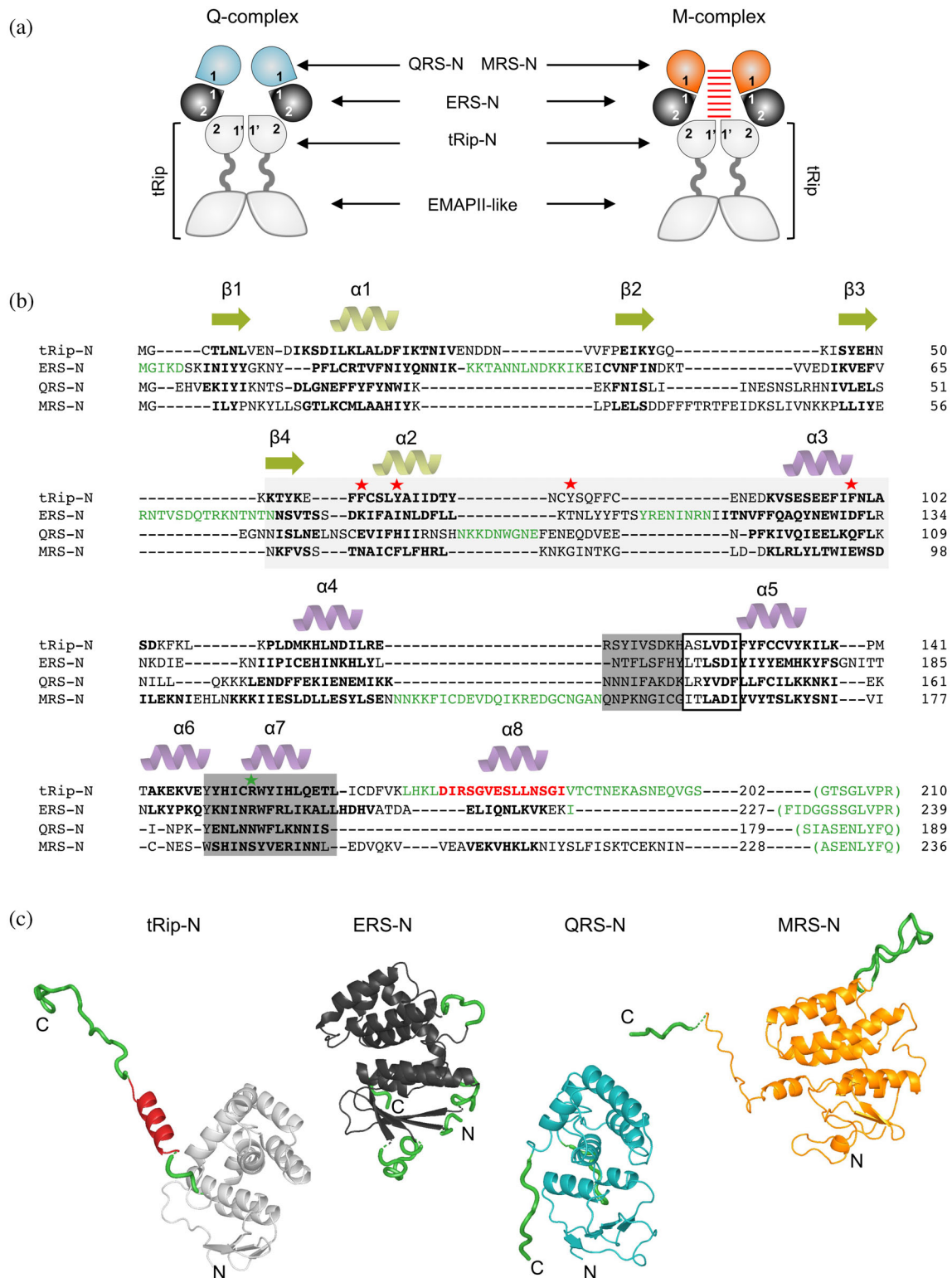(c) tRip-N   ERS-N   QRS-N   MRS-N

FIGURE 1 Legend on next page.

release from the MSC (Arif et al., 2009; Cui et al., 2021; Frechin et al., 2014; Quevillon et al., 1997); these alternative functions are crucial for the cell (reviewed in [Guo & Schimmel, 2013; Lee et al., 2009; Park et al., 2010]). Although different in size and composition, eukaryotic MSCs assembly follows a dominant strategy involving mainly domains with homology to glutathione transferases (GST-like), which interact via two well identified binding surfaces referred to as interfaces 1 and 2 (Cho et al., 2015; Cho

et al., 2019; Karanasios et al., 2007; Simader, Hothorn, Köhler, et al., 2006).

The nuclear genome of the malaria parasite *Plasmodium* codes for a single AIMP, that was named tRip for tRNA import protein. (Bour et al., 2016) Three aaRSs interacting specifically with tRip were identified by co-immunoprecipitation: ERS, QRS, and MRS. All MSC proteins possess N-terminal GST-like domains (tRip-N, ERS-N, QRS-N, and MRS-N) and their association was characterized in vitro by combining mutagenesis, pull-down assays, and light scattering approaches. (Jaramillo Ponce et al., 2022) The results suggested that, unlike other eukaryotic organisms, *Plasmodium* has two independent MSCs that differ in their biophysical features. Specifically, we showed that the tRip strongly associates with ERS-N (via interface 2) to form the common core for both MSCs. Then, either the QRS or MRS associate with this tRip:ERS-N core (via interface 1), leading to the generation of two mutually exclusive heterotrimeric MSCs (tRip:ERS-N:QRS-N and tRip-N:ERS-N:MRS-N) with a stoichiometry of 2:2:2 (Figure 1a). These complexes were named Q-complex and M-complex, respectively. Not only the interaction networks that link the GST-like domains of ERS to QRS or to MRS are driven by different sets of residues, but also only the M-complex tends to oligomerize in vitro. However, tRip is a very unusual AIMP in terms of its localization and function. On the one hand, it is the only AIMP known to date anchored to the plasma membrane with a C-terminal tRNA-binding module (EMAPII-like domain) exposed outside the parasite. On the other hand, it has been shown that *Plasmodium* sporozoites, the infectious form of the parasite delivered to the vertebrate host by mosquito bites, can import exogenous tRNAs in vitro. This import is tRip-dependent and stimulates parasite development at the blood stage.

In this study, we investigated the four GST-like domains of the *Plasmodium* MSCs by combining the crystal structures of *P. vivax* tRip-N (Gupta et al., 2020) and *P. berghei* ERS-N (this study) with size-exclusion chromatography small-angle x-ray scattering (SEC-SAXS) analysis to understand how they are assembling in the tRip:ERS core and in both the M- and Q-complexes.

2 | RESULTS

2.1 | Modeling of GST-like domains of the *P. berghei* MSCs

Multi sequence analysis and structure modeling with ColabFold (Mirdita et al., 2022) and RaptorX identified the presence of a GST-like domain in all 4 proteins belonging to the *P. berghei* MSCs: tRip-N, ERS-N, QRS-N, and MRS-N (Figures S1 and S2). These domains are conserved in all *Plasmodium* species and in other *Apicomplexan* lineages like *Toxoplasma* (van Rooyen et al., 2014). RaptorX provided more compact models and the top templates used to model the GST-like domains are shown in Figure S2a. Interestingly, the GST-like domains of tRip and of the aaRSs were not modeled with the same set of templates. tRip-N was modeled using predominantly GST-like structures of aaRSs, elongation factors or AIMPs. Alternatively, the N-termini of the three *Plasmodium* aaRSs (ERS-N, QRS-N, and MRS-N) were modeled based mainly on different types of catalytically active GST enzymes. Despite their low sequence identity (<25%; Figure 1b), all of them adopt a GST-like structure,

FIGURE 1 GST-like domains and initially proposed association in *Plasmodium* multi-synthetase complexes (MSCs). (a) Association of GST-like domains (drop shape) in the *P. berghei* MSCs based on data from (Jaramillo Ponce et al., 2022a). The central tRip dimer (alternative interface 1′, gray) binds 2 monomers of ERS-N (black) via interface 2, which in turn interact with 2 molecules of QRS-N (cyan) or MRS-N (orange) via interface 1, yet with different strategies. Contrary to QRS-N, optimal binding of MRS-N requires the presence of the dimeric tRip bound to ERS-N (red lines). (b) Structural alignments of the 4 GST-like domains involved in the formation of *P. berghei* MSCs. β-strands and α-helices are indicated with bold residues as they were delineated in the crystal structures of *P. vivax* tRip-N (Gupta et al., 2020) and ERS-N (this study) as well as in the RaptorX models of QRS-N and MRS-N. Unstructured loops and terminal extensions are shown in green: tRip-N (residues 170–173; 188–210), ERS-N (residues 1–4; 32–44; 66–80; 108–115; 227–239), QRS-N (residues 76–84; 180–189), MRS-N (residues 127–149; 229–236). For cloning constraints, a glycine residue was added downstream of the initiator methionine but is not considered for the numbering of the following amino acids. The crystal structure of *P. vivax* tRip-N included residues 1–174, thus the presence of helix α8 (in red) was deduced from ColabFold modeling (Figures S1 and S3a). The GST-like interfaces 1 and 2 are indicated with light and dark gray boxes, respectively. The conserved hydrophobic amino acids involved in the alternative interface 1′ of tRip are indicated with red stars and the arginine residue involved in interface 2 formation between tRip-N and ERS-N is shown with a green star. The N-capping box and hydrophobic staple motif (Φ-S/T-X-X-D-Φ), which are crucial for the stability of the domain (Aceto et al., 1997; Dragani et al., 1997) are boxed in helix α5. (c) Structural models of the different recombinant GST-like domains. The model of *P. berghei* tRip-N (gray) displays the additional residues 175–202 containing helix α8 (red) that are modeled ab initio with CORAL (Petoukhov et al., 2012) in our SAXS analysis. The crystal structure of ERS-N (black) and RaptorX models of QRS-N (Cyan) and MRS-N (orange) are also shown. All of them contain flexible segments which are indicated in green (indicated also in b).
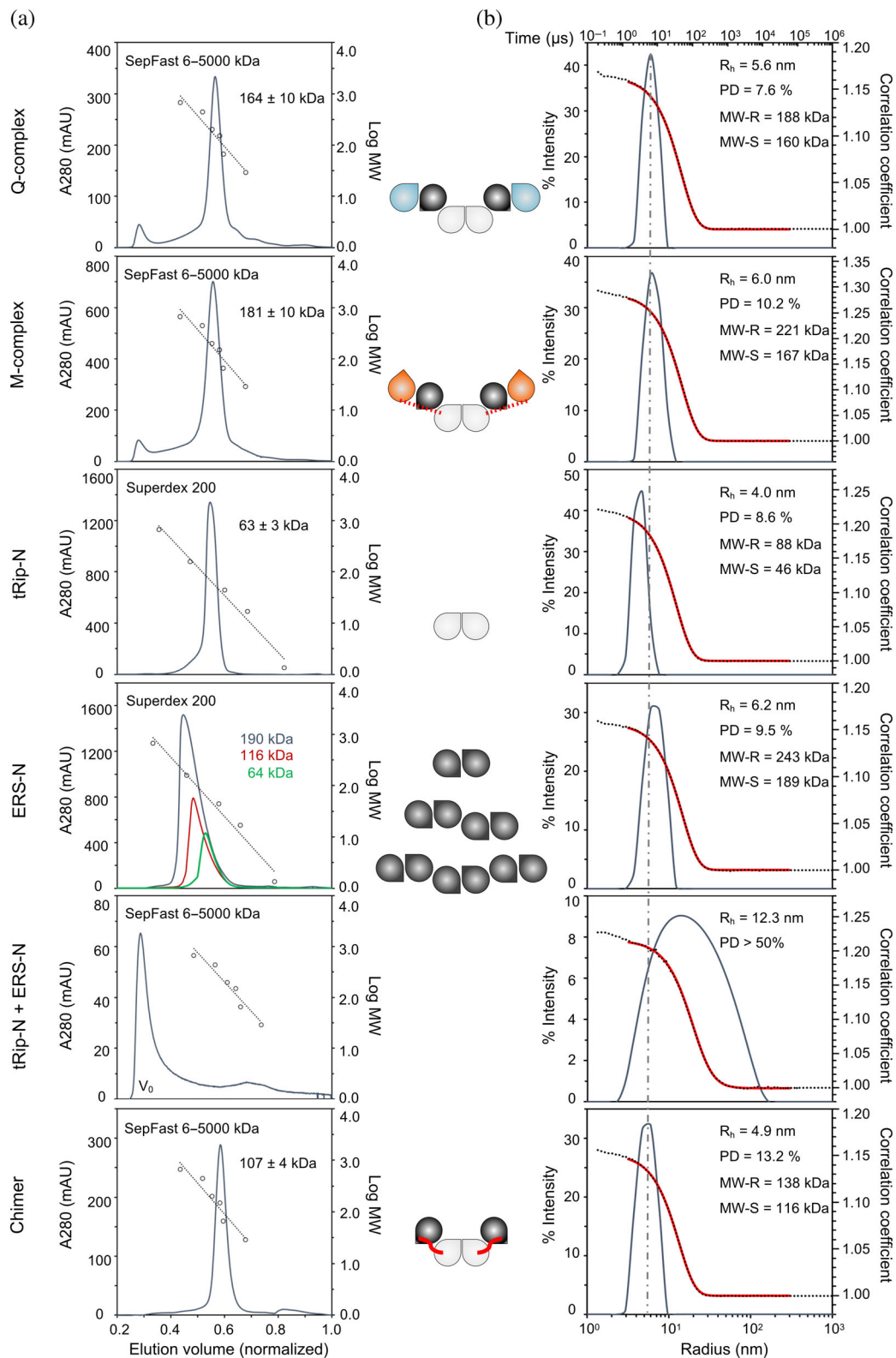
FIGURE 2 Legend on next page.

which consists of 4 β-strands and 2 α-helices that define the N-terminal thioredoxin-like subdomain and a bundle of 5 or 6 α-helices that constitute the C-terminal subdomain (Figure 1b). The reliability of these models for low-resolution studies was validated by the following

observations: the RaptorX predictions of *P. berghei* tRip-N and ERS-N showed good agreement with the subsequently solved crystal structures, the RaptorX and Colab-Fold models of QRS-N overlap decently and the MRS-N model was very similar to the GST-like domain of the

human MRS, yet absent from the RaptorX templates (Figure S2b).

The model of the *P. berghei* tRip-N displays residues 174–202, absent from the crystal structure of the *P. vivax* homologous protein (Gupta et al., 2020), this sequence would contain an eighth helix (174–187) (Figures 1c and S3). Moreover, the GST-like domains exhibit unstructured loops and terminal extensions, which were considered flexible and modeled ab initio as dummy atoms with CORAL during SAXS analysis (Figure 1b,c).

2.2 | Design of recombinant proteins and complex purification

Several constructions with and without a 6-His tag attached at the C-terminus of the GST-like domains were designed. tRip-N and ERS-N were expressed efficiently in *Escherichia coli* as soluble proteins (Figure S4a). QRS-N and MRS-N were also well expressed but their solubilities were limited (Jaramillo Ponce et al., 2022). Therefore, another set of fusion proteins was produced in which a cleavable SUMO module was added to the C-terminus of QRS-N and MRS-N to increase their solubility (Figure S4a). These fusion proteins were then used as efficient baits in M- and Q-complexes purifications (Figure S4b); These complexes were reconstituted by co-lysis of bacteria expressing tRip-N, ERS-N, and either QRS-N-SUMO-6His (Q-complex) or MRS-N-SUMO-6His (M-complex) and purified by Ni-NTA-affinity and size exclusion chromatography (SEC).

2.3 | Size determination of the Q- and M-complexes

The SEC profiles confirmed that the purified Q- and M-complexes were soluble (Figure 2a). Both complexes eluted as a unique peak in the SepFast column with apparent MW of 164 and 181 kDa, respectively. Those values were compatible with a unique population of particles, characterized by a 2:2:2 stoichiometry as demonstrated in (Jaramillo Ponce et al., 2022). The eluted SEC samples were characterized by dynamic and static light scattering (DLS and SLS) to obtain an accurate measurement of the size distribution of these particles (Figure 2b). Cumulant analysis of DLS data yielded a hydrodynamic radius (R_h) of 5.6 nm for the Q-complex and 6.0 nm for the M-complex, both with low percentages of polydispersity (PD), indicating that the samples were homogeneous. The MW derived from DLS (MW-R), which assumes spherical particles, was larger than the shape-independent SLS estimate (MW-S), suggesting particles with rather elongated shapes.

2.4 | Purification of the tRip-N:ERS-N subcomplex, the scaffold of the M- and Q-complexes

The two *Plasmodium* MSCs share a common core formed by the association of tRip-N and ERS-N. tRip-N (24.5 kDa) elutes as a single peak in SEC with an apparent MW of 63 kDa (Figure 2a). Similarly, batch DLS/SLS indicated homogenous samples with MW-R of 88 kDa and MW-S of 46 kDa (Figure 2b), thus suggesting dimers of tRip-N with an elongated shape (MW-R > MW-S). The oligomeric state of *P. berghei* tRip-N in solution is consistent with the dimeric crystal structure of *P. vivax* tRip-N. However, its extended shape is likely due to the 28 C-terminal additional residues present in our construct (Figure 1b,c).

In contrast, the ERS-N domain showed a particular behavior during the purification process. First, it precipitated at low salt concentrations, however, this precipitation was reversible. In addition, during the Ni-NTA-affinity chromatography, a washing step with a gradient

FIGURE 2 Homogeneity and apparent size of purified protein samples. (a) SEC chromatograms. Individual domains or complexes were analyzed on Superdex 200 (10/300) or SepFast (6–5000 kDa) columns, respectively. Each graph shows an elution profile (left y-axis) and a calibration curve (right y-axis). Calibration is based on the elution of thyroglobulin (669 kDa), γ-globulin (158 kDa), ovalbumin (44 kDa), myoglobin (17 kDa), and vitamin B12 (1.35 kDa) on the Superdex 200 column and of thyroglobulin (669 kDa), apoferritin (443 kDa), β-amylase (200 kDa), alcohol dehydrogenase (150 kDa), bovine serum albumin (66 kDa), and carbonic anhydrase (29 kDa) on the SepFast column. The apparent MWs (MW) calculated from the calibration curve are indicated ($n \geq 3$). Only ERS-N has a concentration-dependent apparent MW: 64, 116, and 190 kDa at 2, 6, and 12 mg/ml, respectively. (b) Particle size distribution. The intensity-based particle size distribution (left y-axis) is shown as a function of particle radius (lower x-axis); The experimental data (black dots) and the cumulants-fitted autocorrelation function (red line) is represented on the right y-axis as a function of time (upper x-axis). In each case, the percentage of polydispersity of the distribution (PD), the hydrodynamic radius (R_h), and the corresponding MWs estimated by DLS (MW-R) and SLS (MW-S) are indicated. Measurements were performed at 2 mg/ml of the chimeric protein, 2.4 mg/ml of Q- and 2.1 mg/ml of M- complexes, while individual domains were tested at higher concentrations: 9.7 mg/ml of tRip-N, 8.6 mg/ml of ERS-N, and 7 mg/ml of each tRip-N + ERS-N. The schematic representation of each particle is shown in the middle.

of NaCl was necessary to remove nucleic acid contaminations. This nonspecific binding of nucleic acids was attributed to the high isoelectric point of ERS-N ($pI = 9.38$). Furthermore, on the SEC column, the elution volume of the protein was dependent on its initial concentration (Figure 2a). At 2 mg/ml, ERS-N (28.55 kDa) appeared as a dimer (apparent MW = 64 kDa), but at higher concentrations (4 and 12 mg/ml), the protein eluted earlier with apparent MW of 116 and 190 kDa, respectively, indicating sequential association of ERS-N molecules to form larger oligomeric assemblies in solution. This was confirmed by DLS/SLS (Figure 2b) with MW-R and MW-S of 243 and 189 kDa, respectively in concentrated samples (8 mg/ml), suggesting the presence of elongated hexamers.

Surprisingly, although tRip-N and ERS-N are stable in solution individually, when mixed, they eluted together in the SEC void volume (V$_0$; Figure 2a). DLS measurements indicated that aggregation occurs rapidly upon mixture as the size-distribution becomes wider (PD > 50%) after a few minutes (Figure 2b). Similarly, copurification of the two domains also produced proteins that precipitate promptly after elution from the Ni-NTA affinity column. Numerous conditions were tested to solubilize the tRip-N:ERS-N complex (e.g., pH, salt concentration, glycerol, and detergents), but none of them yielded convincing results.

2.5 | Design and characterization of a chimeric tRip-N:ERS-N

A fusion of tRip-N and ERS-N into a single chimeric protein was made to prevent aggregation. Several constructs were engineered and expressed in *E. coli* (Figure S5a), but only those in which tRip-N was fused at the N-terminus of ERS-N showed solubility. The size of the linker between the two proteins was not important as long as the C-terminal sequence of tRip-N covered amino acids 180–202. They probably act as a flexible linker which is sufficient to accommodate the ERS-N moiety in the fusion without steric hindrance. The chimeric protein (52.57 kDa) eluted with an apparent MW of 107 kDa on SEC (Figure 2a) indicating that it dimerizes in solution. This soluble dimeric state was confirmed by DLS and SLS with a low PD (Figure 2b). The protein did not precipitate and remained homogenous for several days at 4°C. Functionally, the chimeric protein behaved like individual tRip-N and ERS-N in pull-down experiments and interacted with both MRS-N or QRS-N in solution (Figure S5b). It is therefore most likely that this chimera reconstitutes the tRip-N:ERS-N scaffold of the Q- and M-complexes.

2.6 | Crystallization and x-ray diffraction (XRD) characterization

The Q- and M- complexes as well as tRip-N, ERS-N, and the chimeric protein were all characterized in DLS by narrow size distributions with percentage of PD low enough to be considered as monodispersed (Figure 2b), and thus suitable for crystallization assays. Of all crystallization tests performed, the only domain that yielded results was the ERS-N, regardless its dynamic behavior in solution. Crystals of ERS-N were directly grown in ammonium sulfate containing glycerol for cryo-protection. Several native data sets were collected, the best diffracted at 2.7 Å resolution. However, despite the availability of several crystal structures of ERS GST-like domains (i.e., Cho et al., 2015, 2019; Simader, Hothorn, Köhler, et al., 2006; Simader, Hothorn, & Suck, 2006), molecular replacement was unsuccessful. To address the phase problem, crystals derivatized with the crystallophore Tb-Xo4® were prepared. Although these crystals diffracted at best at 3.1 Å resolution, multiple data sets with high redundancy could be collected and merged to solve the structure (Table S1 and Figure S6). The final native model does contain five monomers in the asymmetric unit (AU), sulfate, glycerol, and water molecules.

2.7 | Crystal structure of *P. berghei* ERS-N

As expected from sequence analysis ERS-N shows a globular shape and adopts a GST-fold (Figure 3a). The N-terminal thioredoxin-like subdomain displays a twisted four-stranded mixed β-sheet (β1–β4) flanked by two α-helices (α1 and α2). The C-terminal subdomain is made of α-helices (α3–α8), all of them oriented parallel to each other, except for the helix α7. Superimposition with the GST-like domains of *S. cerevisiae* ERS (PDB 2HRA) and *H. sapiens* ERS (PDB 5A1N) showed a well conserved fold (Figure S6). Several residues located in loops or at the termini of the protein were not visible in the electron density and are likely flexible (highlighted in green in Figures 1b,c).

The asymmetric unit of the crystal contains five molecules of ERS-N (Figure 3b). Two dimers of ERS-N (B:C and D:E) form an elongated tetramer (B:C:D:E) that binds a fifth molecule (A). Three types of interfaces were observed (Figure 3c). Dimerization of B:C and D:E involve interface 1; In each dimer, the two subunits are related by a two-fold rotation with helices α2 and α3 of one monomer interacting with helices α3 and α2 of the second monomer in a parallel orientation. The area of this interface is ~1200 Å^2 and is similar to the GST-like

(a)

(b)

(c)

Interface 1
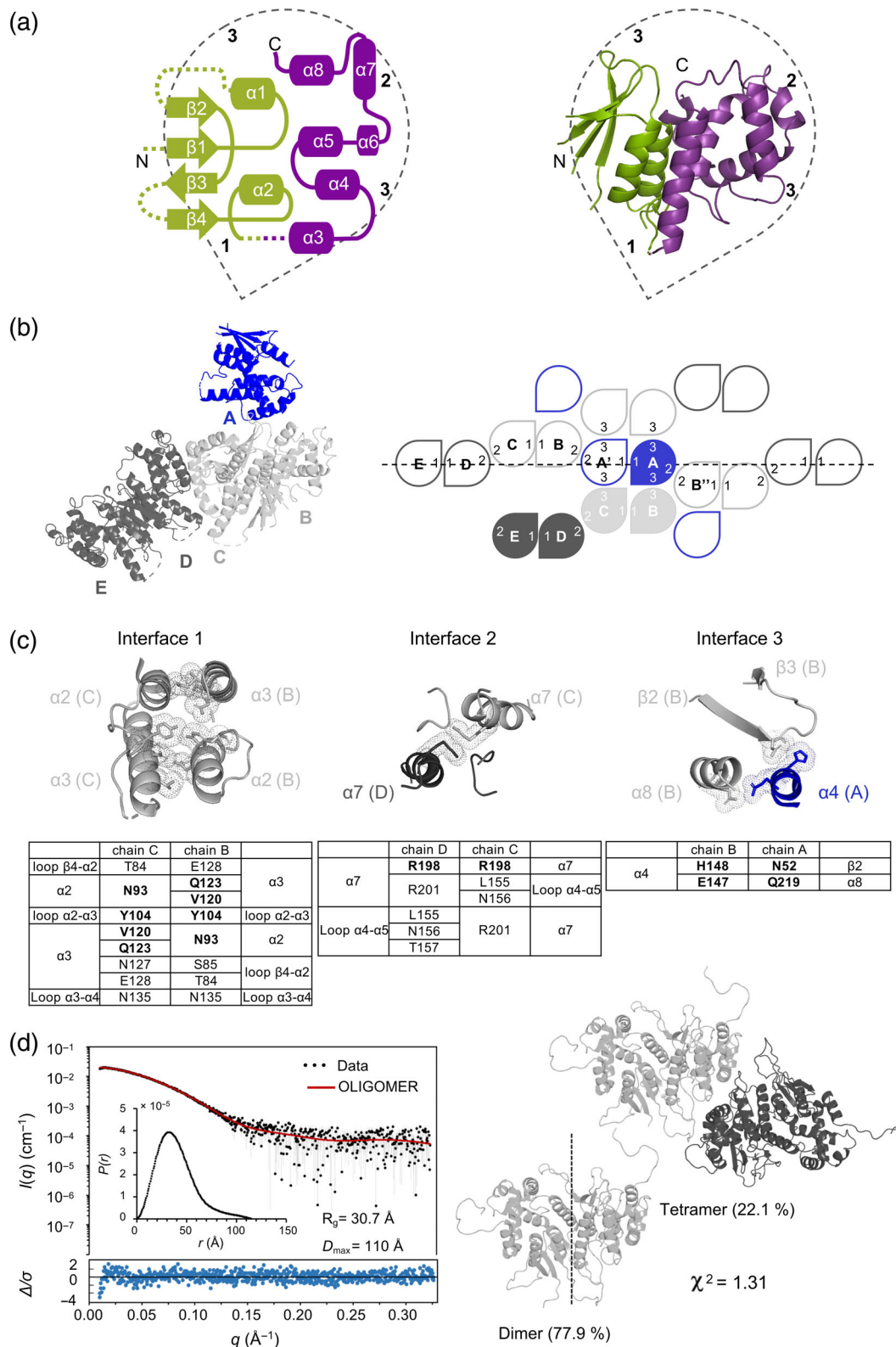
	chain C	chain B	
loop β4-α2	T84	E128	α3
α2	N93	Q123	
		V120	
loop α2-α3	Y104	Y104	loop α2-α3
α3	V120	N93	α2
	Q123		
	N127	S85	loop β4-α2
	E128	T84	
Loop α3-α4	N135	N135	Loop α3-α4

Interface 2

		chain D	chain C	
α7		R198	R198	α7
		R201	L155	Loop α4-α5
			N156	
Loop α4-α5		L155	R201	α7
		N156		
		T157		

Interface 3

		chain B	chain A	
α4		H148	N52	β2
		E147	Q219	α8

(d)

Data
OLIGOMER

R_g= 30.7 Å
D_{max} = 110 Å

Tetramer (22.1 %)

χ^2 = 1.31

Dimer (77.9 %)

FIGURE 3 Legend on next page.

heterodimerization observed in the human MRS:AIMP3 (PDB 4BVX) and EPRS:AIMP2 (PDB 5A1N) subcomplexes. (Cho et al., 2015) Subunits C and D interact through interface 2, involving helix α7 and the loop between helices α4 and α5. The two monomers are also related by a two-fold rotation axis and the interface of ∼780 Å^2 is characterized by a π-stacking interaction between two strictly conserved arginines (Figure 3c). This

interface is similar to those observed in the crystal of *P. vivax* tRip-N (PDB 5ZKF chains C and D) (Gupta et al., 2020) and in ERS:AIMP interactions in the yeast (Simader, Hothorn, Köhler, et al., 2006) and human (Cho et al., 2015) MSCs. The insertion of the fifth ERS-N molecule (A) is driven by an asymmetric interface 3 ($\sim$380 Å^2), involving helix α4 of subunit A and both the helix α8 and the loop between strands β2 and β3 of subunit B (Figure 3c). The same interaction is observed between subunit C and A′ of an adjacent asymmetric unit, which lead to an alternative tetramer (C:B:A:A′) (Figure 3b) with a combined interface of $\sim$760 Å^2. ERS-N molecules form continuous helicoidal fibers around five-fold screw axes, which are linked to each other by interfaces 3.

2.8 | SEC-SAXS analysis

SEC-SAXS was used to characterize the size and shape of molecular assemblies observed in solution (Figure 2) and to propose atomic models (Figures 3–5) for the different components of *Plasmodium* MSCs based on crystal structures of *P. berghei* ERS-N (this study) and *P. vivax* tRip-N (Gupta et al., 2020), as well as RaptorX models of *P. berghei* QRS-N and MRS-N (Figure 1c). Details of experimental conditions and structural parameters such as radii of gyration (R_g), maximum dimensions (D_{max}), estimates of molecular weight (MW), molecular compactness derived from the analysis of Guinier plots, pair-distance distributions *P(r)*, or Kratky plots are summarized in Table S2 and Figure S7.

2.8.1 | Solution structure of ERS-N

The SEC-SAXS analysis of ERS-N revealed steadily decreasing values of R_g and MW along the elution peak (Figure S7a). This was consistent with the observation of a variation of size as a function of concentration in SEC (Figure 2) and with the propensity of ERS-N to self-associate and form a mixture of various oligomers. ERS-N oligomerization was then investigated with OLIGOMER (Konarev et al., 2003), which revealed that the combination of 77.9% of dimers B:C and 22.1% of tetramers B:C:D:E as observed in the crystal structure (Figure 3b) best fitted the SAXS data (Figure 3d, Table S2).

2.8.2 | Solution structures of tRip-N and tRip-N-ERS-N chimera

Both samples were highly homogeneous (Figure 2), and R_g and MW analysis confirmed the presence of dimeric particles (Figure 4; Table S2, Figure S7a). In both cases, two models were built in which tRip-N homodimerization occurs either through (i) a canonical interface 1 as in the dimer of ERS-N or (ii) the unusual alternative GST-like interface 1′ observed in the *P. vivax* crystal structure (PDB 5ZKE). In an ensemble (*n* = 20) of models generated with CORAL for tRip-N, the latter interface yielded slightly better fits to the experimental SAXS data and both models were characterized by extended conformations of their C-termini (Figure 4a, Table S2), suggesting some degree of flexibility (Figure S7c). The tRip-N construct included 28 additional amino acids, containing the predicted helix

FIGURE 3 Crystal structure of ERS-N. (a) Topological diagram and cartoon representation of ERS-N. The thioredoxin subdomain (residues 1–100, β1-α1-β2-β3-β4-α2) is colored green and the C-terminal helical subdomain is colored purple (residues 101–240, α3–α8). All secondary structures (α-helices and β-strands) are identified, and the N- and C-terminal ends are indicated. Segments not visible in the electron density are indicated with dotted lines in the topological diagram. The drop shape of the GST-like domains and the different interfaces are highlighted. (b) Arrangement of the different asymmetric units (ASU) in the crystal. The ASU contains five molecules of ERS-N (A:B:C:D:E). Two canonical GST-like dimers (B:C and D:E) involving interface 1 interact via their interface 2 (C:D) to form a tetramer, and the 5th molecule (A) binds subunit B using an asymmetric interface 3. Molecules A from two adjacent ASUs form a dimer (A:A′) via interface 1 and the two other ASUs using interfaces 2. Molecules interact alternatively by interfaces 1 and 2 and form helical fibers around a five-fold axis (dashed line). (c) Interfaces between ERS-N molecules in the ASU. Three types of interactions were observed. Residues involved in the formation of the main interactions are highlighted with sticks and dots. Interface 1: Two ERS-N monomers form a canonical GST dimer by interacting along α2 and α3 helices between the B and C monomers (or D and E). Interface 2: Dimerization occurs through α7 helices between monomers C and D (or A and B) where two characteristic arginine residues are stacked on top of each other. Interface 3: This interaction is restricted to this study and involves α8 and β2 of the A chain and α4 from the B chain. Tables summarize the main interactions between GST-like domains, including hydrogen bonds identified by PDBePISA (Krissinel & Henrick, 2007); residues highlighted in the crystal structures above are shown in bold. (d) SAXS data of ERS-N. Experimental data (black dots) are superimposed with the theoretical curve (red) of a mixture of dimers (B:C) and tetramers (B:C:D:E) of ERS-N calculated with OLIGOMER. The pair-distance distribution function *P(r)* and the derived radius of gyration (R_g) and particle maximum dimension (D_{max}) are shown in the inset. The error-weight residuals of the OLIGOMER fit are shown below the graph. In the structures, the dimerization interface 1 of ERS-N is indicated with a dashed line.
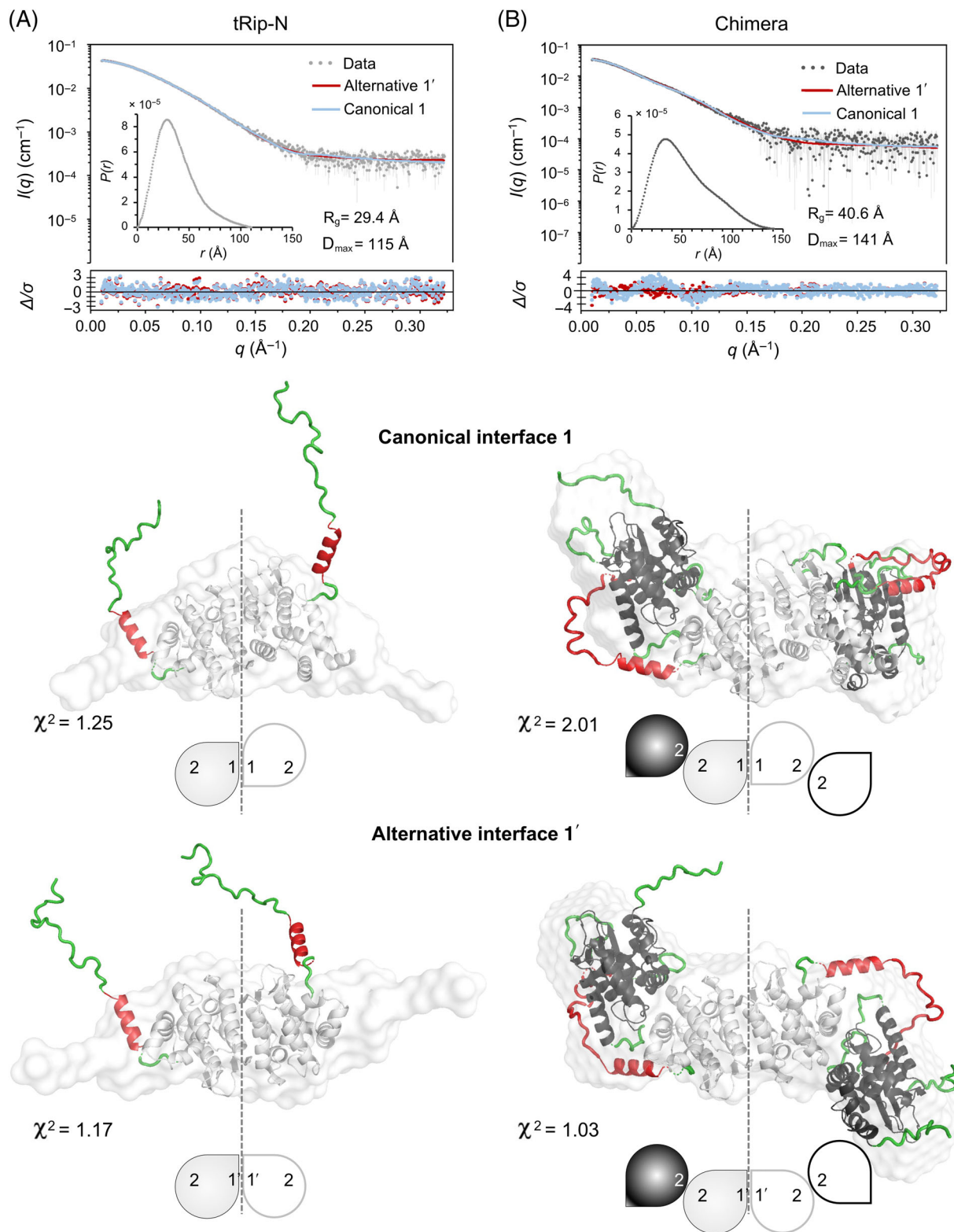
FIGURE 4 Legend on next page.

α8 followed by a stretch of disordered residues (Figures 1b and S2a), which were all modeled ab initio.

This C-terminal tail of tRip-N was long enough to link tRip-N and ERS-N in the chimera, with the two

GST-like domains interacting through their interfaces 2. CORAL was used to generate models, treating the domains as rigid bodies while reconstructing ab initio their linker and loops missing in the crystal structure of

ERS-N (Figure 1b). As for tRip-N, the two possible interfaces 1 were tested in the modeling of the chimera. All reconstructions ($n = 20$) with the alternative GST-like dimerization of tRip-N provided excellent fits to the experimental SAXS data ($\chi^2 = 0.97$–1.04) (Figure 4b). On the contrary, when tRip-N was constrained to dimerize through a canonical interface 1, the fits were significantly poorer ($\chi^2 = 2.33$–2.75).

These results unambiguously confirmed that the alternative interface 1′ is used for tRip-N homodimerization in solution and is not an artifact of crystallization or a specificity of *P. vivax* tRip-N.

2.8.3 | Structure solutions of Q- and M-complexes

Both complexes eluted as a single peak, but were overlapped by small amounts of higher oligomers, especially in the M-complex (Figure 5; Figure S7a). Despite these heterogeneities, we could obtain SAXS curves corresponding to monodisperse samples (Figure S7b) and the derived MWs supported a 2:2:2 stoichiometry (Table S2). Models of the Q-complex generated with CORAL readily provided good fits to the experimental data ($n = 20$, $\chi^2 = 1.25$–1.33; Figure 5a, Table S2). With ColabFold, the predicted model appeared very similar but with a weaker fit ($\chi^2 = 2$) to the SAXS data (Figure S8a), validating thus the proposed quaternary structure of the Q-complex: the QRS-N associates with the tRip-N:ERS-N subcomplex (Figure 4b) by binding interface 1 of ERS-N. In contrast, using the same strategy, all models generated with CORAL for the M-complex fitted the data less well (Figure S8b), strongly suggesting a different positioning of the GST-like domains. Indeed, different domain orientations in the M and Q complexes are evidenced by differences in $P(r)$ distributions although both complexes share the same equivalent associated subunits (MRS-N or QRS-N). However, ColabFold generated a model highly consistent with the SAXS data but with a different interaction network (Figure S8b). In this model of the M-complex, the center is occupied by an ERS-N homodimer (interface 1) that binds two tRip-N (interface 2) while tRip-N binds

to MRS-N (interface 1). CORAL modeling using such arrangement provided excellent fits to the SAXS curve ($n = 20$, $\chi^2 = 1.01$–1.06; Figure 5b, Table S2).

### 2.9 | Could helix 8 be responsible of the anchoring of tRip at the membrane?

The C-terminal domain of tRip was expressed in Cos7 cells to test its capacity to associate with the membrane fraction. The transfected cells were disrupted, and both the membrane and the soluble fractions were analyzed by Western Blot (Figure 6). Since the *P. berghei* tRip$_{148-402}$ fragment was not expressed (Figure S3b), we used the sequence of the *P. falciparum* protein to test its ability to associate with the cell membrane based on the presence or absence of the α8 helix. Comparison of carbonate versus detergent extraction showed that *P. falciparum* tRip$_{148-402}$ behaves like the calnexin, a reticulum endoplasmic membrane protein. Unlike the soluble GFP, tRip$_{148-402}$ and the calnexin are mostly found in the membrane fraction and are released in the supernatant only after Triton X-100 extraction, and not after lysis or Na$_2$CO$_3$ treatment, suggesting that they are integral membrane proteins. Moreover, deletion of the α8 helix in tRip$_{181-402}$ allows the C-terminal domain to be relocated into the cell cytosol (Figure 6), suggesting that the α8 helix has the potential to associate tRip to cell membranes on its own.

3 | DISCUSSION

Our structural analysis focused on the one hand on the crystal structure of the GST-like N-terminal domain of the *P. berghei* ERS (ERS-N) and on the other hand, on the structures of its related complexes in solution, that is, the *Plasmodium* Q- and M- MSCs and tRip-N:ERS-N subcomplex that forms their respective inner scaffold. (Jaramillo Ponce et al., 2022) As expected, ERS-N disclosed a GST-like fold (Figure 3a), characterized by an oligomeric assembly involving not only the canonical interfaces 1 and 2, but also an additional interface that

---

FIGURE 4 SAXS models of (a) tRip-N and (b) tRip-N-ERS-N chimera. The experimental SAXS data of tRip-N (light gray dots) and the chimeric protein (dark gray dots) are superimposed with the scattering curves of two CORAL models, in which tRip-N homodimerizes either through the canonical interface 1 (light blue) observed in all known GST-like domains, including ERS-N, or through the alternative GST-like interface 1′ (red) detected in the crystal structure of *P. vivax* tRip-N (Gupta et al., 2020). The experimental $P(r)$ and the derived R_g and D_{max} values are shown in the insets. Error-weighted residuals of each CORAL fit to the experimental data (Δ/σ) are displayed below the graph. The corresponding χ^2 values are indicated below the models. Models display rigid bodies of tRip-N (gray) and ERS-N (black) as well as tRip-N helix α8 fused to the linker (red) and flexible segments (green). Homodimerization interfaces are indicated with a dashed line. A refined ab initio bead model (gray surface) selected from cluster analysis is overlaid with each CORAL model for comparison.
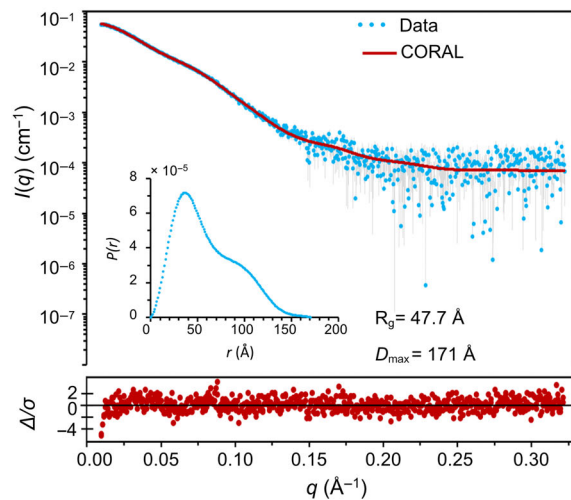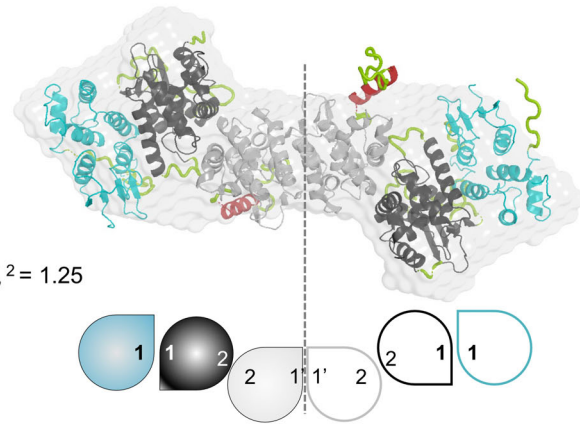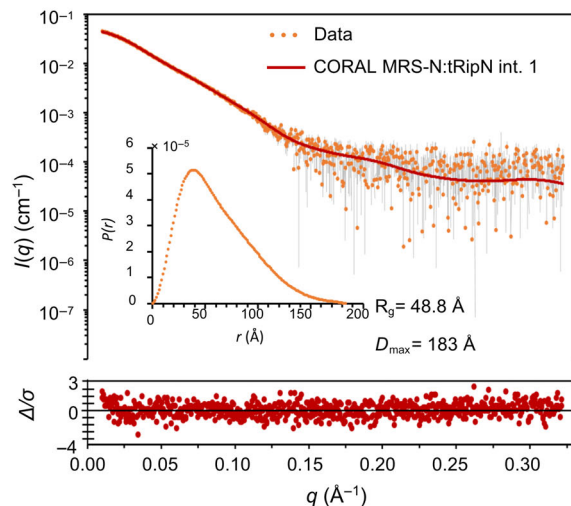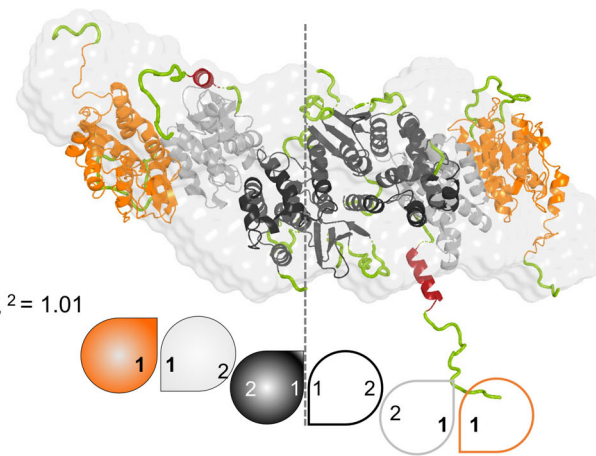
FIGURE 5 SAXS data of the two ternary (a) Q- and (b) M- complexes. The experimental SAXS data of Q- (cyan dots) and M- (orange dots) complexes are superimposed with the theoretical scattering curve of CORAL models (red). The two complexes differ in the interaction network of their components. The Q-complex homodimerizes via the alternative interface 1′ of tRip-N, while the M-complex uses the canonical interface 1 of ERS-N, leading to complexes with distinct shapes, as evidenced by the $P(r)$ functions. Homodimerization interfaces are indicated with a dashed line. More information is detailed in the legend of Figure 4.

allows the integration of a fifth ERS-N molecule into the asymmetric unit of the crystal (Figure 3b). To our knowledge, this additional interface 3 (Figure 3c) has not been observed in other examples of GST-like domain interactions. Although this contact may be an artifact of the crystal packing, we cannot rule out a biologically relevant interface. In contrast, interfaces 1 and 2 as identified in the ERS-N crystal structure are classical interactions present in all crystal structures of *S. cerevisiae* and *H. sapiens* MSC subcomplexes available in the PDB. (Cho et al., 2015; Cho et al., 2019; Simader, Hothorn, Köhler, et al., 2006) For example, in the yeast MSC complex, the AIMP Arc1p interacts with the GST-like domain of MRS

through interface 1 and with the GST-like domain of ERS through interface 2 (Figure 7).

The two M- and Q-complexes of *Plasmodium* are dimers of heterotrimers. They are organized around a subcomplex in which tRip-N binds to ERS-N. Also, the tRip-N:ERS-N subcomplex aggregates rapidly and cannot be purified as is (Figure 2). This behavior can be explained by the ability of ERS-N to oligomerize quickly in solution (Figures 2 and 3c), which has neither been observed with the other 3 GST-like domains that constitute *Plasmodium* MSCs nor with GST-like domains involved in yeast or human MSCs. However, the engineering of a linker between the C-terminus of tRip-N and
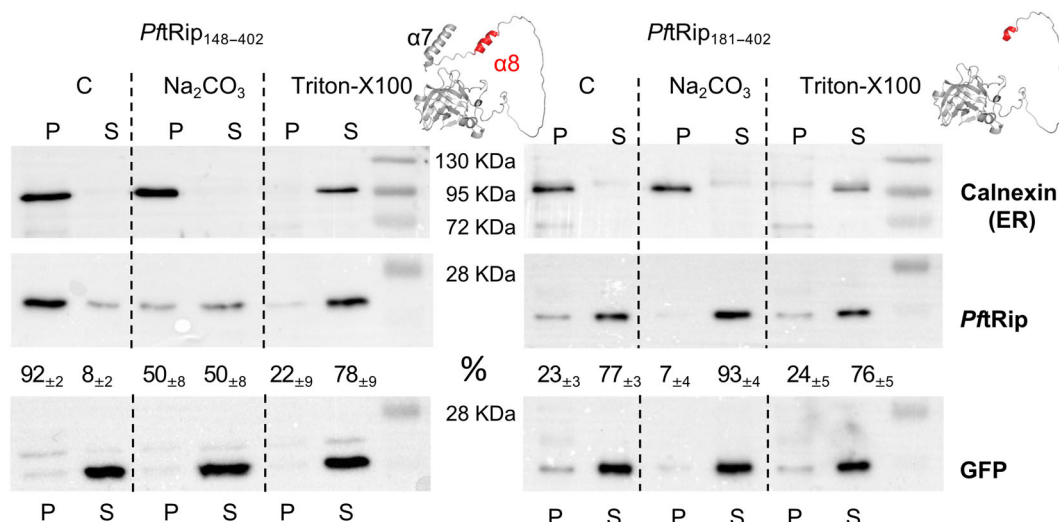
FIGURE 6 Carbonate versus Triton extraction of membrane proteins from mammalian cells expressing *P. falciparum* tRip C-terminal domains. GFP is always present in the soluble fractions (S) while both *Pf*tRip and calnexin (endoplasmic reticulum) were found in the membrane pellet (P) even after Na_2CO_3 treatment and were completely released into the supernatant only upon Triton-X100 treatment. C stands for control, where the cell lysis was performed in the absence of Na_2CO_3 and Triton-X100. The percentage of tRip in each fraction is indicated as the mean $\pm$ standard deviation of four independent experiments. Repeatedly, upon Na_2CO_3 treatment, the total intensity (P + S) of the *Pf*tRip$_{148-402}$ signal is two to three-fold lower than that of the control or the Triton-X-100 samples.

the N-terminus of ERS-N in the chimeric protein (Figure S5a) prevented this phenomenon. This linker allows neutralizing unintended interactions and thus avoids the formation of long chains of tRip-N:ERS-N. Yet, it is flexible enough to enable the chimeric protein to associate with the QRS-N or MRS-N domains (Figure S5b). Remarkably, the chimeric protein also answered a key question about the homodimerization mode of tRip-N. In the crystal structure of *P. vivax* tRip-N, the protein dimerizes through an alternative interface 1′ (PDB 5ZKE). It involves conserved aromatic residues (corresponding to F91, Y55, Y63, and Y72 in the *P. berghei* tRip sequence, Figure 1b) and α2 and α3 helices of each monomer are oriented perpendicularly. The SAXS data of tRip-N (Figure 4a) did not allow to differentiate between this unique dimerization strategy and a canonical interface 1 where α2 and α3 helices of each monomer are parallel (as in the ERS-N crystal). However, only tRip homodimerization using the alternative interface 1′ provides an optimal fit with the SAXS data obtained for the tRip-N:ERS-N chimera protein (Figure 4b). It shows that this unusual dimerization pattern is not a crystallization artifact. Furthermore, it is consistent with the localization and function of tRip on the parasite surface (Bour et al., 2016), since the dimer conformation itself would accommodate for the joint presence of the two EMAPII-like C-terminal domains outside the cell (Figure 7). Moreover, based on its capacity to associate with membranes, we propose that helix

α8 could be responsible for the anchoring of tRip in the plasma membrane (Figure 6).

Even though they are built from similar modules, the two independent MSCs display two very different structural configurations. Indeed, the GST-like domains of *Plasmodium* QRS and MRS are characterized by similar folds, but their association with the tRip-N:ERS-N subcomplex leads to different models (compare Figure 5a,b). The docking guided by the occurrence of a canonical interface 1 between QRS-N and ERS-N is in good agreement with SAXS experimental data. However, this is not the case between MRS-N and ERS-N (Figure S8b). The only modeling of the M-complex that accurately fit the SAXS data shows an unexpected domain organization: the MRS-N domain binds directly tRip-N, causing the tRip-N:ERS-N subcomplex to dimerize via the ERS-N interface 1. This strategy still allows both C-terminal extremity of tRip-N to point toward the same direction (Figures 5b and 7). Moreover, these results explain our previous observations (Jaramillo Ponce et al., 2022) indicating (i) that QRS-N binds directly to ERS-N in the Q-complex while MRS-N requires the presence of the tRip to integrate the M-complex, (ii) that the residues involved in the association of QRS-N and MRS-N to their respective complexes are different, although located on the equivalent surfaces of both molecules, and (iii) that the mutation of residues involved in the formation of the alternative interface 1′ of tRip-N specifically prevents the binding of MRS-N (Figure S9). Not only do the two
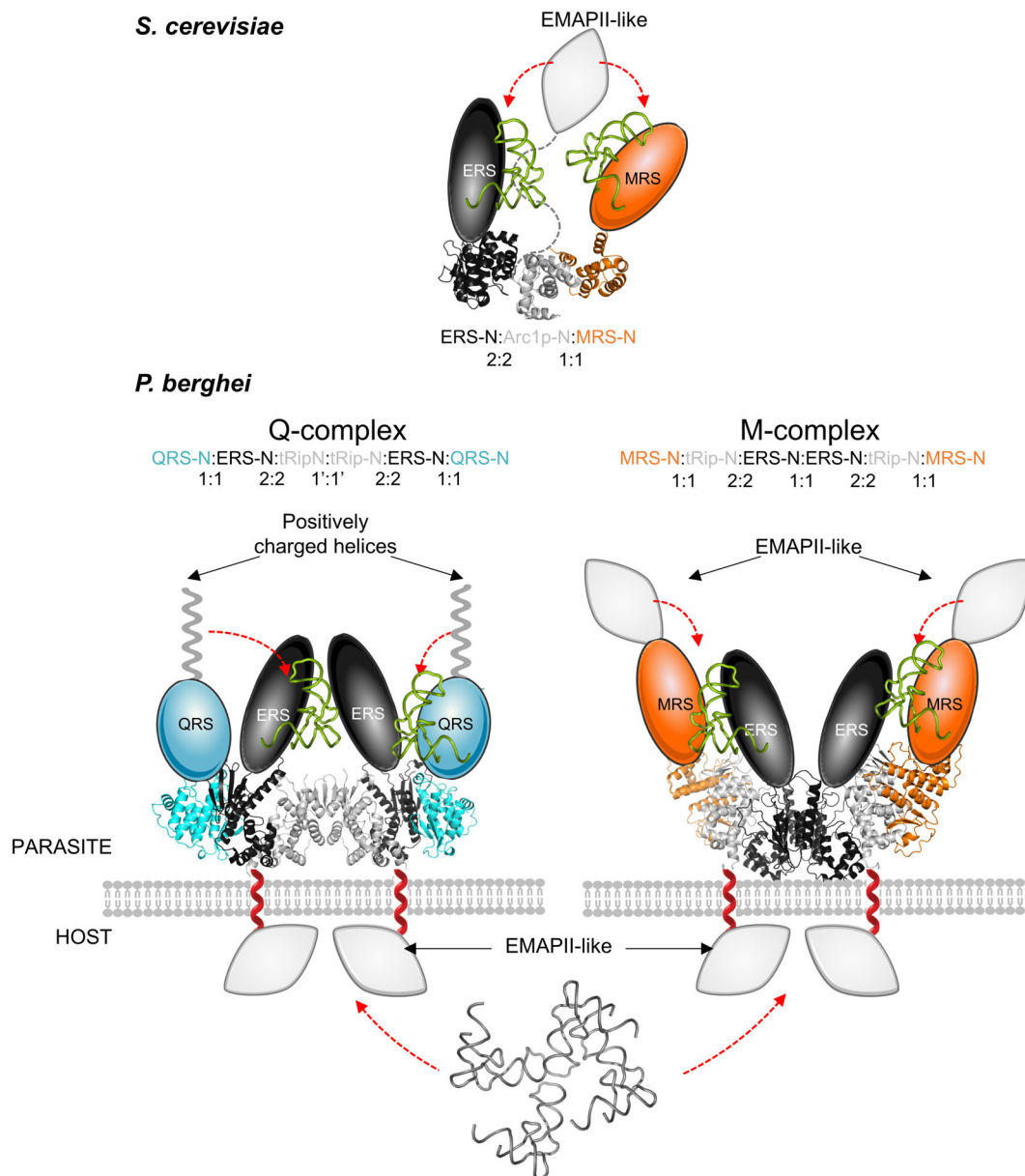
FIGURE 7 Membrane-bound MSC of *P. berghei* compared to cytosolic MSC of yeast. The unique yeast MSC contains the AIMP Arc1p that binds to ERS (interface 2) and MRS (interface 1). The complex is cytosolic and the tRNA binding domain (EMAPII-like) of Arc1p increases the affinity of ERS and MRS for their cognate tRNAs. Alternatively, *Plasmodium* displays two independent MSCs, each containing two copies of membrane-bound tRip, ERS-N, and either QRS-N (Q-complex) or MRS-N (M-complex) but with different configurations. Models of the GST-like interaction domains of yeast Arc1p (1–122), ERS-N (20–196), and MRS-N (59–161) based on crystal structures (PDB 2HRK and 2HSN) and of *P. berghei* tRip-N (1–190), ERS-N (1–204), QRS-N (1–178), and MRS-N (1–196) are shown in ribbon while the ERS, QRS, and MRS cores and the C-terminal tRNA-binding domains of Arc1p, tRip, QRS, and MRS are schematized; The latters correspond either to the EMAPII-like domain in Arc1p, tRip and MRS (gray diamonds) or to a positively charged helix fused to the C-terminus of QRS. *S. cerevisiae* MSC is organized around Arc1p which was shown to be a tRNA aminoacylation co-factor increasing the affinity of both bound ERS and MRS for their cognate tRNA^{Glu} and ^{Met}, respectively (Deinert et al., 2001; Simos et al., 1996). The singular feature of the *Plasmodium* Q- and M- complexes is that tRip is bound to the parasite plasma membrane, with the aaRSs inside and the tRNA-binding domain of tRip exposed to external/host tRNAs. The tRip helix α8 (red) has the capacity to associate with membranes and is shown here as a transmembrane helix. The presence of additional tRNA binding modules fused to the QRS and MRS could compensate for the outside localization of tRip EMAPII domain. The composition of the complexes as well as the interaction interfaces involved are indicated.

specific interaction networks uncovered in this study explain why QRS-N and MRS-N cannot be found in a single complex, but these structural differences also raise

the question of the potential implications of the two *Plasmodium* MSCs in divergent functions. For example, it may be proposed that (i) both the M- and Q- complexes

could, as it is the case for most MSCs known to date, be reservoirs of ERS, QRS and MRS and control their release to perform functions other than tRNA aminoacylation in the cytosol or other cellular compartments (Cui et al., 2021) (ii) whereas only the M-complex, by forming an oligomer in the membrane, could be involved in importing exogenous tRNAs into the parasite.

The protein tRip is the only example known to date of an AIMP with a total uncoupling between the anchoring of aaRSs in an MSC and the tRNA binding function of its C-terminal domain. Indeed, the presence of the membrane barrier between the tRip N-terminal GST-like domain located inside the parasite and the EMAPII domain located outside prevents the latter from participating directly in the aminoacylation reaction. The absence of tRip EMAPII inside the parasite might be compensated by the tRNA binding capacities of the additional domains of QRS (C-terminal positively charged helix) and MRS (C-terminal EMAPII) to increase tRNA affinity as the EMAPII domain of Arc1p does in the single cytosolic yeast complex (Simos et al., 1996; Figure 7). Indeed, the EMAPII domain of Arc1p (monomeric homolog of tRip) has a preference for yeast tRNA^{Met} and tRNA^{Glu} (Deinert et al., 2001) and participates in efficient glutamylation and methionylation in the cell. (Galani et al., 2001) On the contrary, the tRNA specificity of the tRip EMAPII (*H. sapiens* tRNA$^{Leu, Ser, Asn, Ala}$) (Cela et al., 2021) does not correlate with the aaRSs found in the Q- and M-MSCs, suggesting that imported tRNAs play a role beyond their aminoacylation by ERS, MRS and QRS in *Plasmodium* homeostasis.

4 | MATERIALS AND METHODS

4.1 | Bioinformatic analysis

Sequences of *Plasmodium berghei* tRip (PBANKA_1306200), ERS (PBANKA_1362000), QRS (PBANKA_1346600), and MRS (PBANKA_0518700) were used for reference. Multiple sequence alignments were performed using T-Coffee. (Magis et al., 2014) Detection of structural and functional domains was carried out with HHpred (Soding et al., 2005). The identification of related proteins from other organisms was performed using BLASTp and PSI-BLAST (Altschul, 1997). Physical and chemical parameters were calculated with the ProtParam tool from ExPASy (Gasteiger et al., 2005). Secondary structure was predicted using the Quick2D tool (Zimmermann et al., 2018) and three-dimensional models were initially predicted using RaptorX server (Källberg et al., 2012) and more recently AlphaFold2

(Mirdita et al., 2022; Varadi et al., 2022); protein interfaces in crystal structures were analyzed with PDBePISA. (Krissinel & Henrick, 2007) Structural alignments and superimposition of 3D models were performed using the PyMOL (Schrödinger & DeLano, 2020) command "super," which is adapted for proteins with low sequence similarity as the GST-like domains.

4.2 | Plasmid constructions and production of recombinant proteins

Synthetic genes (GenScript) encoding the GST-like domains of *P. berghei* tRip, ERS, QRS, and MRS were cloned into pET15b fused either to a removable C-terminal 6-His tag by thrombin cleavage or a removable SUMO-6His tag by TEV cleavage as indicated in (Jaramillo Ponce et al., 2022). All constructions displayed a glycine insertion after the first methionine derived from the cloning restriction site. To increase protein solubility, sequences were adapted to the human codon usage which allowed to decrease the AT content but retained some rare codons to reduce the translation speed of the bacterial ribosomes. Cultures were performed as described in (Jaramillo Ponce et al., 2022); cultures were started from freshly transformed *E. coli* BL21(DE3) cells and protein expression was induced at low temperature (16°C).

4.3 | Purification of individual proteins

The protocol of purification is detailed in (Jaramillo Ponce et al., 2022). In short, bacteria were disrupted by sonication, the crude extract was ultracentrifuged and loaded onto a Ni-NTA column (Sigma-Aldrich His-Select® HF). In the case of ERS-N, a linear gradient up to 2 M NaCl was added during the wash to remove bound nucleic acids. Eluted protein fractions were pooled and dialyzed overnight at 4°C in the presence of thrombin (GE Healthcare). Cleaved proteins were recovered in the flow-through of a second Ni-NTA column coupled to a 1 ml HiTrapBenzamidine FF column (GE Healthcare) to remove the protease. Fractions were pooled, concentrated and further purified by Size Exclusion Chromatography (SEC) in SEC buffer (25 mM HEPES-NaOH pH 7.0, 300 mM NaCl, 5% (v/v) glycerol, 0.005% (w/v) DDM, 5 mM β-Mercaptoethanol). The protein concentration was determined using the NanoDrop® ND-1000 spectrophotometer (Thermo Fisher Scientific). The quality of the sample was estimated using the A_{260}/A_{280} ratio (about 0.5 for pure protein solutions) and by SDS-PAGE.

4.4 | Reconstitution and purification of complexes

The protocol of purification is detailed in (Jaramillo Ponce et al., 2022). Complexes were reconstituted by cellular "colysis." One pellet of bacteria expressing SUMO-6-His-tagged bait protein and one or two other pellets of bacteria expressing non-tagged prey proteins were mixed and sonicated in ice. Samples were treated in the same manner as for the purification of individual proteins. After affinity purification, the SUMO-6HisTag was removed by digestion with a 6xHis-tagged TEV protease and cleaved proteins were recovered in the flow-through of a second Ni-NTA column.

Interactions between *P. berghei* QRS-N and MRS-N with the chimeric protein (Figure S4b), were investigated by in vitro pull-down assays as described in (Jaramillo Ponce et al., 2022).

4.5 | Size-exclusion chromatography (SEC)

Individual proteins (tRip-N and ERS-N) were injected onto a Superdex 200 Increase 10/300 column (GE Healthcare) while the chimeric protein and complexes ($\geq$100 kDa) were purified on a SepFast SEC 6–5000 kDa column (BioToolomics). SEC columns were run with the same SEC buffer (25 mM HEPES-NaOH pH 7.0, 300 mM NaCl, 5% (v/v) glycerol, 0.005% (w/v) DDM, 5 mM β-ME) and were periodically calibrated either with Bio-Rad's gel filtration standard (#1511901) or MWGF1000 kit (Sigma-Aldrich), respectively, to determine molecular weight (MW) estimates from the chromatograms. In addition, blue dextran was used to determine the column's void volume (V_0).

4.6 | Dynamic and static light scattering (DLS/SLS)

Light scattering measurements were performed in a 1 μl quartz cuvette on a DynaPro Nanostar instrument from Wyatt Technology (Santa Barbara, CA) as described in (Jaramillo Ponce et al., 2022). Prior to measurements, samples were ultracentrifuged at 4°C during 1 h at 100,000g (S45A rotor in a Sorvall Hitachi Discovery M150SE micro-ultracentrifuge) and the sample concentration was verified on a NanoDrop ND-1000 spectrophotometer (Thermo Fisher Scientific).

4.7 | Crystallization of ERS-N

ERS-N-$_{6His}$ (10 mg/ml in SEC buffer) was ultracentrifuged at 100,000g for 1 h at 4°C. Crystallization experiments were performed in 96-well sitting-drop plates (CrystalQuick® X, Greiner Bio-One) using a Mosquito nanoliter pipetting robot (TTP Labtech, UK). Commercial kits, Crystal Screen HT (Hampton Research) and JBSscreen JCSG++ (Jena Bioscience), were used to determine initial crystallization conditions (200 nl drops, 1:1 drop ratio). Spherulites were obtained in 2 M ammonium sulfate and 100 mM Bis-Tris pH 5.5. Conditions were first optimized by testing ammonium sulfate concentration, additives, pH and temperatures. Small crystals (<50 μm) diffracting only at 5 Å (Swiss Light Source, Villigen, Switzerland) were obtained at 25°C in 1.4–1.5 M ammonium sulfate, 100 mM HEPES-NaOH pH 7.5 and 0.5% (v/v) PEG. Further optimization was achieved through microseed matrix screening as described in (D'Arcy et al., 2007; D'Arcy et al., 2014). Optimal crystals (> 100 μm) were obtained in 1.4–1.5 M ammonium sulfate, 100 mM HEPES-NaOH pH 7.5 and 20% (v/v) glycerol after 2–3 weeks at 25°C.

4.8 | XRD data collection and structure determination of ERS-N

Native crystals were either directly flash frozen in liquid nitrogen or incubated for 2 min with terbium derivatives (1 μl of 100 mM Tb-Xo4® dissolved in 1.6 M ammonium sulfate, 100 mM HEPES-NaOH pH 7.5, 20% (v/v) glycerol) prior to cryocooling. (Engilberge et al., 2017) x-ray diffraction data were collected on PROXIMA-1 beamline at SOLEIL Synchrotron (Saint-Aubin, France) using an EIGER-X 16 M detector (Dectris Ltd.). Native data sets were collected at a wavelength λ = 0.9786 Å with an oscillation range of 0.1° over 360°. Three single-wavelength anomalous dispersion (SAD) data sets were collected from one derivative crystal close to the terbium L_{III} absorption edge (λ = 1.6314 Å) with an oscillation range of 0.1° over 720° to increase multiplicity. Initial phases allowed to choose a clear hand solution (mean FOM of 0.53). Five monomers per asymmetric unit were partially built (1010 residues out of 1245, FOM = 0.89) using automated model building combined with additional density modification. Further details on this experimental phasing are given in Figure S6. Both *Shelx* (Schneider & Sheldrick, 2002; Sheldrick, 2008) and *Solomon* (Abrahams & Leslie, 1996) were the only combination within this pipeline that resulted in interpretable electronic density maps and the resulting model was refined to R_{work} of 19.2% and R_{free} of 23.7% (Table S1). This initial model was used in refinement cycles against a native protein dataset using the *Phenix* software package (Liebschner et al., 2019) and *Coot*. Data processing and data collection statistics are summarized in Figure S6 and Table S1, respectively.

4.9 | Size-exclusion chromatography coupled to small-angle x-ray scattering (SEC-SAXS)

SEC-SAXS data were collected on the SWING beamline at the SOLEIL synchrotron (Saint-Aubin, France). Prior to x-ray exposure, samples were separated on a Bio SEC-3 column (4.6 × 300 nm, 300 Å, Agilent) equilibrated with SEC buffer at 0.2 ml/min. Details of data collection and processing are shown in Table S2 and Figure S7. All data sets were treated using a q-range of 0.01–0.33 ($q_{min} < \pi/D_{max}$). Correction for capillary fouling was applied when necessary. (Brookes et al., 2016) The quality of the SAXS curves was assessed with Guinier, $P(r)$ and MW analyses. The ambiguity of the scattering data dictated the use of symmetry restraints and cluster analysis for ab initio 3D reconstructions. For each data set, 20 bead models with P2 symmetry were generated, clustered, averaged and further refined. Table S2 only shows the statistics of a selected cluster, which was more consistent with the proposed atomic models. MODELER 10.1 (Webb et al., 2014) was used to add the missing loops in ERS-N for OLIGOMER analysis and to build a model of dimeric *P. berghei* tRip-N based on the PDB 5ZKE (Gupta et al., 2020), imposing an α-helix structure for residues 174–187 (Figure 1b). The model of tRip-N dimerizing through a canonical interface 1 was constructed by superimposition with the ERS-N dimer (chains A and A′). The heterodimer tRip-N:ERS-N was constructed using a model of *P. berghei* tRip-N based on the PDB 5ZKF (Gupta et al., 2020) and the chains C and D of the crystal structure of ERS-N. Superimposition of tRip-N with one of these molecules of ERS-N reconstitutes an interface 2 with the characteristic stacking of arginines in helices α7. Integration of QRS-N or MRS-N in the complexes through a canonical interface 1 was modeled based on the ERS-N dimer. For CORAL hybrid modeling, the different subunits in the chimer and the Q- and M-complexes were split into several rigid bodies delimited by the flexible segments indicated in Figure 1b. All of them, except for tRip-N helix α8, were kept fixed during simulating annealing and the remaining residues were modeled as dummy atoms. For each analysis, 20 calculations were performed. Hybrid models and refined bead models were superimposed using *SUPCOMB*. (Kozin & Svergun, 2001) Alternatively, models were obtained with ColabFold using (i) the model of the *P. berghei* tRip-N dimer based on PDB 5ZKE, (ii) the crystal structure of the *P. berghei* ERS-N monomer, and (iii) QRS-N or MRS-N models taken from ColabFold predictions of *P. berghei* QRS and MRS, respectively (Figure S1) as building blocks.

4.10 | Construction mammalian expression vectors, transfection carbonate versus detergent assay and Western blot

DNA sequences encoding tRip (148–402) and tRip (181–402) either from *P. berghei* or *P. falciparum* were introduced into pCI-neo vector for expression in mammalian cells. COS-7 cells were cultured at 37°C with 5% CO_2 in DMEM GlutaMAX growth medium (Life Technologies) containing 4.5 mg/L glucose, 50 U/ml penicillin, 50 µg/ml streptomycin and 10% fetal calf serum. They were transfected with pCI-neo constructs and pCDNA3.1-GFP as a control, using the jetOPTIMUS transfection reagent according to the manufacturer's instructions (Polyplus transfection). After 24 h incubation, cells were washed with PBS 1X (Life Technologies) and collected for further investigations. Cell lysis was achieved by three freezing and thawing cycles, in 5 mM Tris–HCl pH 8.0, in 0.1 M Na_2CO_3 pH 11.5 or in 5 mM Tris–HCl pH 8.0 containing 1% (v/v) Triton X-100. Samples were incubated 30 min on ice before centrifugation (15 min at 15,000g). Pellets and soluble fractions were then separated on 10% SDS-PAGE and transferred to PVDF membrane (Millipore) and analyzed by Western Blot with specific antibodies raised against *Pf*tRip (214–402). (Bour et al., 2016).

DATA AVAILABILITY STATEMENT

Data openly available in a public repository that issues datasets with DOIs.

ORCID

Magali Frugier https://orcid.org/0000-0002-8079-5303

REFERENCES

Abrahams JP, Leslie AGW. Methods used in the structure determination of bovine mitochondrial F1 ATPase. Acta Crystallogr D Biol Crystallogr. 1996;52:30–42.

Aceto A, Dragani B, Melino S, Allocati N, Masulli M, Ilio CD, et al. Identification of an N-capping box that affects the α6-helix propensity in glutathione S-transferase superfamily proteins: a role for an invariant aspartic residue. Biochem J. 1997;322:229–34.

Altschul S. Gapped BLAST and PSI-BLAST: a new generation of protein database search programs. Nucleic Acids Res. 1997;25: 3389–402.

Arif A, Jia J, Mukhopadhyay R, Willard B, Kinter M, Fox PL. Two-site phosphorylation of EPRS coordinates multimodal regulation of noncanonical translational control activity. Mol Cell. 2009;35:164–80.

Bour T, Mahmoudi N, Kapps D, Thiberge S, Bargieri D, Ménard R, et al. *Apicomplexa*-specific tRip facilitates import of exogenous tRNAs into malaria parasites. Proc Natl Acad Sci U S A. 2016; 113:4717–22.

Brookes E, Vachette P, Rocco M, Pérez J. *US-SOMO* HPLC-SAXS module: dealing with capillary fouling and extraction of pure component patterns from poorly resolved SEC-SAXS data. J Appl Cryst. 2016;49:1827–41.

Cela M, Théobald-Dietrich A, Rudinger-Thirion J, Wolff P, Geslain R, Frugier M. Identification of host tRNAs preferentially recognized by the *Plasmodium* surface protein tRip. Nucleic Acids Res. 2021;49:10618–29.

Cho HY, Lee HJ, Choi YS, Kim DK, Jin KS, Kim S, et al. Symmetric assembly of a decameric subcomplex in human multi-tRNA synthetase complex via interactions between glutathione transferase-homology domains and aspartyl-tRNA synthetase. J Mol Biol. 2019;431:4475–96.

Cho HY, Maeng SJ, Cho HJ, Choi YS, Chung JM, Lee S, et al. Assembly of multi-tRNA synthetase complex via heterotetrameric glutathione transferase-homology domains. J Biol Chem. 2015;290:29313–28.

Cui H, Kapur M, Diedrich JK, Yates JR, Ackerman SL, Schimmel P. Regulation of ex-translational activities is the primary function of the multi-tRNA synthetase complex. Nucleic Acids Res. 2021;49:3603–16.

D'Arcy A, Bergfors T, Cowan-Jacob SW, Marsh M. Microseed matrix screening for optimization in protein crystallization: what have we learned? Acta Crystallogr F Struct Biol Commun. 2014;70:1117–26.

D'Arcy A, Villard F, Marsh M. An automated microseed matrix-screening method for protein crystallization. Acta Crystallogr D Biol Crystallogr. 2007;63:550–4.

Deinert K, Fasiolo F, Hurt EC, Simos G. Arc1p organizes the yeast aminoacyl-tRNA synthetase complex and stabilizes its interaction with the cognate tRNAs. J Biol Chem. 2001;276:6000–8.

Dragani B, Stenberg G, Melino S, Petruzzelli R, Mannervik B, Aceto A. The conserved N-capping box in the hydrophobic core of glutathione S-transferase P1–1 is essential for refolding. J Biol Chem. 1997;272:25518–23.

Engilberge S, Riobé F, Di Pietro S, Lassalle L, Coquelle N, Arnaud C-A, et al. Crystallophore: a versatile lanthanide complex for protein crystallography combining nucleating effects, phasing properties, and luminescence. Chem Sci. 2017;8:5909–17.

Frechin M, Enkler L, Tetaud E, Laporte D, Senger B, Blancard C, et al. Expression of nuclear and mitochondrial genes encoding ATP synthase is synchronized by disassembly of a multisynthetase complex. Mol Cell. 2014;56:763–76.

Galani K, Großhans H, Deinert K, Hurt EC, Simos G. The intracellular location of two aminoacyl-tRNA synthetases depends on complex formation with Arc1p. EMBO J. 2001;20:6889–98.

Gasteiger E, Hoogland C, Gattiker A, Duvaud S, Wilkins MR, Appel RD. Bairoch a protein identification and analysis tools on the ExPASy server. In: Walker JM, editor. The proteomics protocols handbook. Totowa, NJ: Humana Press; 2005. p. 571–607. https://doi.org/10.1385/1-59259-890-0:571

Guo M, Schimmel P. Essential nontranslational functions of tRNA synthetases. Nat Chem Biol. 2013;9:145–53.

Guo M, Yang, XL. Architecture and metamorphosis. In: Kim, S, editor. Aminoacyl-tRNA synthetases in biology and medicine. Dordrecht: Springer; 2013. p. 89–118. https://doi.org/10.1007/128_2013_424

Gupta S, Chhibber-Goel J, Sharma M, Parvez S, Harlos K, Sharma A, et al. Crystal structures of the two domains that constitute the Plasmodium vivax p43 protein. Acta Crystallogr D Struct Biol. 2020;76:135–46.

Havrylenko S, Mirande M. Aminoacyl-tRNA synthetase complexes in evolution. Int J Mol Sci. 2015;16:6571–94.

Jaramillo Ponce JR, Kapps D, Paulus C, Chicher J, Frugier M. Discovery of two distinct aminoacyl-tRNA synthetase complexes anchored to the plasmodium surface tRNA import protein. J Biol Chem. 2022;298:101987.

Källberg M, Wang H, Wang S, Peng J, Wang Z, Lu H, et al. Template-based protein structure modeling using the RaptorX web server. Nat Protoc. 2012;7:1511–22.

Kang T, Kwon NH, Lee JY, Park MC, Kang E, Kim HH, et al. AIMP3/p18 controls translational initiation by mediating the

delivery of charged initiator tRNA to initiation complex. J Mol Biol. 2012;423:475–81.

Karanasios E, Simader H, Panayotou G, Suck D, Simos G. Molecular determinants of the yeast Arc1p–aminoacyl-tRNA synthetase complex assembly. J Mol Biol. 2007;374:1077–90.

Konarev PV, Volkov VV, Sokolova AV, Koch MHJ, Svergun DI. *PRIMUS*: a windows PC-based system for small-angle scattering data analysis. J Appl Cryst. 2003;36:1277–82.

Kozin MB, Svergun DI. Automated matching of high- and low-resolution structural models. J Appl Cryst. 2001;34:33–41.

Krissinel E, Henrick K. Inference of macromolecular assemblies from crystalline state. J Mol Biol. 2007;372:774–97.

Kyriacou SV, Deutscher MP. An important role for the multienzyme aminoacyl-tRNA synthetase complex in mammalian translation and cell growth. Mol Cell. 2008;29:419–27.

Laporte D, Huot JL, Bader G, Enkler L, Senger B, Becker HD. Exploring the evolutionary diversity and assembly modes of multi-aminoacyl-tRNA synthetase complexes: lessons from unicellular organisms. FEBS Lett. 2014;588:4268–78.

Lee YS, Shibata Y, Malhotra A, Dutta A. A novel class of small RNAs: tRNA-derived RNA fragments (tRFs). Genes Dev. 2009;23:2639–49.

Liebschner D, Afonine PV, Baker ML, Bunkóczi G, Chen VB, Croll TI, et al. Macromolecular structure determination using X-rays, neutrons and electrons: recent developments in *Phenix*. Acta Crystallogr D Struct Biol. 2019;75:861–77.

Magis C, Taly J-F, Bussotti G, Chang J-M, Di Tommaso P, Erb I, et al. T-Coffee: tree-based consistency objective function for alignment evaluation. Methods Mol Biol. 2014;1079:117–29. https://doi.org/10.1007/978-1-62703-646-7_7

Mirdita M, Schütze K, Moriwaki Y, Heo L, Ovchinnikov S, Steinegger M. ColabFold: making protein folding accessible to all. Nat Methods. 2022;19:679–82.

Park SG, Choi E-C, Kim S. Aminoacyl-tRNA synthetase-interacting multifunctional proteins (AIMPs): a triad for cellular homeostasis. IUBMB Life. 2010;62:296–302.

Petoukhov MV, Franke D, Shkumatov AV, Tria G, Kikhney AG, Gajda M, et al. New developments in the *ATSAS* program package for small-angle scattering data analysis. J Appl Cryst. 2012;45:342–50.

Quevillon S, Agou F, Robinson J-C, Mirande M. The p43 component of the mammalian multi-synthetase complex is likely to be the precursor of the endothelial monocyte-activating polypeptide II cytokine. J Biol Chem. 1997;272:32573–9.

Rubio Gomez MA, Ibba M. Aminoacyl-tRNA synthetases. RNA. 2020;26:910–36.

Schneider TR, Sheldrick GM. Substructure solution with *SHELXD*. Acta Crystallogr D Biol Crystallogr. 2002;58:1772–9.

Schrödinger L, DeLano W. PyMOL. 2020. Available from: http://www.pymol.org/pymol

Sheldrick GM. A short history of *SHELX*. Acta Crystallogr A Found Crystallogr. 2008;64:112–22.

Simader H, Hothorn M, Köhler C, Basquin J, Simos G, Suck D. Structural basis of yeast aminoacyl-tRNA synthetase complex formation revealed by crystal structures of two binary sub-complexes. Nucleic Acids Res. 2006;34:3968–79.

Simader H, Hothorn M, Suck D. Structures of the interacting domains from yeast glutamyl-tRNA synthetase and tRNA-aminoacylation and nuclear-export cofactor Arc1p reveal a novel function for an old fold. Acta Crystallogr D Biol Crystallogr. 2006;62:1510–9.

Simos G, Segref A, Fasiolo F, Hellmuth K, Shevchenko A, Mann M, et al. The yeast protein Arc1p binds to tRNA and functions as a cofactor for the methionyl- and glutamyl-tRNA synthetases. EMBO J. 1996;15:5437–48.

Soding J, Biegert A, Lupas AN. The HHpred interactive server for protein homology detection and structure prediction. Nucleic Acids Res. 2005;33:W244–8.

van Rooyen JM, Murat J-B, Hammoudi P-M, Kieffer-Jaquinod S, Coute Y, Sharma A, et al. Assembly of the novel five-component apicomplexan multi-aminoacyl-tRNA synthetase complex is driven by the hybrid scaffold protein Tg-p43. PLoS One. 2014;9:e89487.

Varadi M, Anyango S, Deshpande M, Nair S, Natassia C, Yordanova G, et al. AlphaFold protein structure database: massively expanding the structural coverage of protein-sequence space with high-accuracy models. Nucleic Acids Res. 2022;50:D439–44.

Webb B, Lasker K, Velázquez-Muriel J, Schneidman-Duhovny D, Pellarin R, Bonomi M, et al. Modeling of proteins and their assemblies with the integrative modeling platform. Methods Mol Biol. 2014;1091:277–95. https://doi.org/10.1007/978-1-62703-691-7_20

Zimmermann L, Stephens A, Nam S-Z, Rau D, Kübler J, Lozajic M, et al. A completely reimplemented MPI bioinformatics toolkit with a new HHpred server at its Core. J Mol Biol. 2018;430:2237–43.

SUPPORTING INFORMATION

Additional supporting information can be found online in the Supporting Information section at the end of this article.